Wavelength-Dependent Photolysis of i-Pentanal and t-Pentanal from 280 to 330 nm

Lei Zhu,* Thomas Cronin, and Amarjit Narang

Wadsworth Center, New York State Department of Health, Department of Environmental Health and Toxicology, State University of New York, Albany, New York 12201-0509

Received: May 10, 1999; In Final Form: July 26, 1999

Photodissociation of i-pentanal ($(CH_3)_2CHCH_2CHO$; 3-methylbutanal) and t-pentanal ($(CH_3)_3CCHO$; 2,2-dimethylpropanal) in the 280−330 nm region was investigated at 5 nm intervals by using dye laser photolysis in combination with cavity ring-down spectroscopy. Absorption cross-sections of i-pentanal and t-pentanal were obtained. Both aldehydes exhibited a broad absorption band peaking at 295 nm, with maximum absorption cross-sections of $(5.90 \pm 0.22) \times 10^{-20}$ and $(4.26 \pm 0.07) \times 10^{-20}$ cm^2, respectively, for i-pentanal and t-pentanal. The formation yield of the HCO radical from photolysis of i-pentanal and t-pentanal was determined by monitoring HCO absorption at 613.8 nm. Except for 325 and 330 nm photolysis of i-pentanal, the HCO yield was found to be independent of aldehyde pressure (2−12 Torr) and total pressure (20−400 Torr). For the photodissociation of t-pentanal, the HCO yield was also determined in the 0.5−2 Torr range and was found to increase with t-pentanal pressure. The variation of HCO radical yield with photolysis wavelength was determined. The peak HCO yields from t-pentanal and i-pentanal photolysis were 0.92 ± 0.11 and 0.40 ± 0.08 at 315 nm, respectively, where uncertainty reflects experimental scatter only. The difference in the peak HCO yield from t-pentanal and i-pentanal photolysis was attributed to the opening up of the Norrish II channel for i-pentanal. End products from closed-cell photolysis of i-pentanal and t-pentanal were investigated at 290, 310, and 330 nm by using HPLC. Acetaldehyde was found to be a product from the photodissociation of i-pentanal/N_2 mixtures. Photolysis rates of i-pentanal and t-pentanal to form HCO were calculated for two representative atmospheric conditions (noontime at sea level and 40° N latitude on January 1 and on July 1) and were compared to those obtained from acetaldehyde photolysis.

Introduction

The photodissociation of aliphatic aldehydes is an important source of HO_2 radicals in the polluted atmosphere.[1−4] These HO_2 radicals can react with NO to form NO_2 and thus participate in tropospheric ozone formation. In a recent paper,[5] we reported the HCO formation yield from the photolysis of n-pentanal ($CH_3(CH_2)_3CHO$) as a function of wavelength in the 280−330 nm range, and estimated the radical formation rate constants for a representative set of atmospheric conditions. Studying the wavelength-dependent photolysis of constitutional isomers of n-pentanal such as i-pentanal ($(CH_3)_2CHCH_2CHO$; 3-methylbutanal) and t-pentanal ($(CH_3)_3CCHO$; 2,2-dimethylpropanal) allows us to examine the effect of alkyl substitution on aldehyde photodissociation product channels and quantum yields.

Aliphatic aldehydes display a weak absorption band in the 240−360 nm region arising from a dipole forbidden n→π^* transition localized on the CO chromophore.[6,7] Based on calculated enthalpy changes from known heats of formation,[8−10] photoexcitation of i-pentanal and t-pentanal can lead to the following possible decomposition pathways:

$$\mathrm{RCHO} + h\nu \rightarrow \mathrm{R} + \mathrm{HCO} \qquad (1)$$

where $\Delta H_{298}{}^0 = 351.0$ kJ·mol^{-1} for R = i-C_4H_9 ($\lambda \leq 340$ nm) and $\Delta H_{298}{}^0 = 342.9$ kJ·mol^{-1} for R = t-C_4H_9 ($\lambda \leq 348$ nm);

$$\mathrm{RCHO} + h\nu \rightarrow \mathrm{CO} + \mathrm{RH} \qquad (2)$$

where $\Delta H_{298}{}^0 = -8.2$ kJ·mol^{-1} for R = i-C_4H_9 and $\Delta H_{298}{}^0 = 4.9$ kJ·mol^{-1} for R = t-C_4H_9 ($\lambda \leq 24.4$ μm);

$$\mathrm{RCHO} + h\nu \rightarrow \mathrm{CH_3CHO} + \mathrm{CH_2{=}CHCH_3} \qquad (3)$$

where $\Delta H_{298}{}^0 = 90.3$ kJ·mol^{-1} ($\lambda \leq 1324$ nm); and

$$\mathrm{RCHO} + h\nu \rightarrow \mathrm{RCO} + \mathrm{H} \qquad (4)$$

where $\Delta H_{298}{}^0 = 365.7$ kJ·mol^{-1} ($\lambda \leq 327$ nm).

Pathways 1 and 2 are radical and molecular fragmentation channels, respectively. Pathway 3, also called the Norrish II process, is only available for i-pentanal. Pathway 4 was found to be minor for small aldehydes.[6] In the absence of literature values of heat of formation for i-C_4H_9CO and t-C_4H_9CO, the enthalpy change for channel 4 was assumed to be the same as that from the photolysis of propionaldehyde. Since channel 4 involves the breaking of a carbonyl hydrogen bond in the photolysis of i-pentanal and t-pentanal as it does in the photolysis of propionaldehyde, such an assumption is reasonable.

Previously published work on t-pentanal[11] and i-pentanal[12] was limited to steady-state photolysis using a full mercury arc. Quantum yields, $\phi_1/\phi_{\mathrm{total}} \approx \phi_2/\phi_{\mathrm{total}} \approx 0.5$, were reported for t-pentanal. The relative quantum yield, $\phi_3/(\phi_1+\phi_2) \approx 0.7$, was obtained for i-pentanal.

In the present study, we report the determination of the wavelength-dependent photodissociation of i-pentanal and t-pentanal in the range 280−330 nm. Photolysis studies were performed at 5 nm intervals. Absorption cross-sections of i- and t-pentanal were determined. The HCO radical yields were measured by using a sensitive detection technique, cavity ring-down spectroscopy.[13,14] The absolute HCO concentrations were

10.1021/jp991540p CCC: $18.00
Published on Web 08/19/1999

calibrated relative to those obtained from formaldehyde photolysis at each wavelength. In addition, we have estimated product yields from the closed-cell photodissociation of i-pentanal and t-pentanal in nitrogen at 290, 310, and 330 nm by using HPLC.

Experimental Section

The experimental apparatus has been described in detail elsewhere.[5,15,16] Tunable photolysis radiation was provided by a frequency-doubled dye laser pumped by a 308 nm XeCl excimer laser (~180 mJ/pulse). Laser dyes used to cover this spectral range were Coumarin 153, Rhodamine 6G, Rhodamine B, Rhodamine 101, Sulforhodamine 101, and DCM. The excimer-pumped dye laser produced an energy output of 10−25 mJ/pulse depending upon the laser dye used and the wavelength studied. Frequency doubling of the fundamental dye laser output yielded 0.9−2.5 mJ/pulse of UV light. After passing through beam turning prisms and mirror, the energy entering the photolysis cell was about 0.6−1.6 mJ/pulse. The photodissociation laser pulse propagated into the reaction cell at a 15° angle with the main cell axis through a sidearm, while the probe laser pulse (613−616 nm) from a nitrogen-pumped dye laser was directed along its main optical axis. The photolysis beam and the probe beam were overlapped at the center of the reaction cell vacuum-sealed with a pair of high reflectance (~99.999% at 614 nm) cavity mirrors. A fraction of the probe laser output was injected into the cavity through the front mirror. The photon intensity decay inside the cavity was monitored by measuring the weak transmission of light through the rear mirror with a photomultiplier tube (PMT). The PMT output was amplified, digitized, and transferred to a computer. The decay curve was fit to a single-exponential decay function and the total loss per optical pass was calculated. By measuring cavity losses with and without a photodissociation pulse, HCO absorption from the photolysis of i-pentanal and t-pentanal was determined. Absorption spectra were obtained by scanning the wavelength of the probe laser with a digital drive unit. The photolysis laser pulse energy was measured with a calibrated Joulemeter.

Gas pressures at the center of the reaction cell were monitored with a Baratron capacitance manometer. Pressures of 2−12 Torr and 0.5−12 Torr were used for i-pentanal and t-pentanal, respectively, in the experiments. Quantum yield measurements were undertaken at a laser repetition rate of 0.1 Hz to ensure replenishment of the gas sample between successive laser shots. Spectrum scans were performed at a repetition rate of 1 Hz. All experiments were carried out at an ambient temperature of 293 ± 2 K.

Analysis of the closed cell photolysis products was done by HPLC using a Hewlett-Packard 1100 Series Chemstation HPLC. The gas products were derivatized on Waters SEP-PAK silica−DNPH cartridges. The derivatized samples were eluted by 5 mL aliquots of acetonitrile and then transferred to sample vials for HPLC analysis. Injection volume of the eluents was 20 μL per sample vial.

i-Pentanal (≥97%) and t-pentanal (≥97%) are liquids at room temperature and were obtained from Aldrich Chemical Co. They were purified by repeated freeze−pump−thaw cycles at 77 and 273 K, respectively. Formaldehyde was generated by the pyrolysis of polymer paraformaldehyde (Aldrich Chemical Co.; ≥95% purity) at 110 °C.[17] Nitrogen (≥99.999% purity, UHP grade) was used as buffer gas and was obtained from Praxair. Oxygen (≥99.994% purity, UHP grade) was purchased from MG Industries.

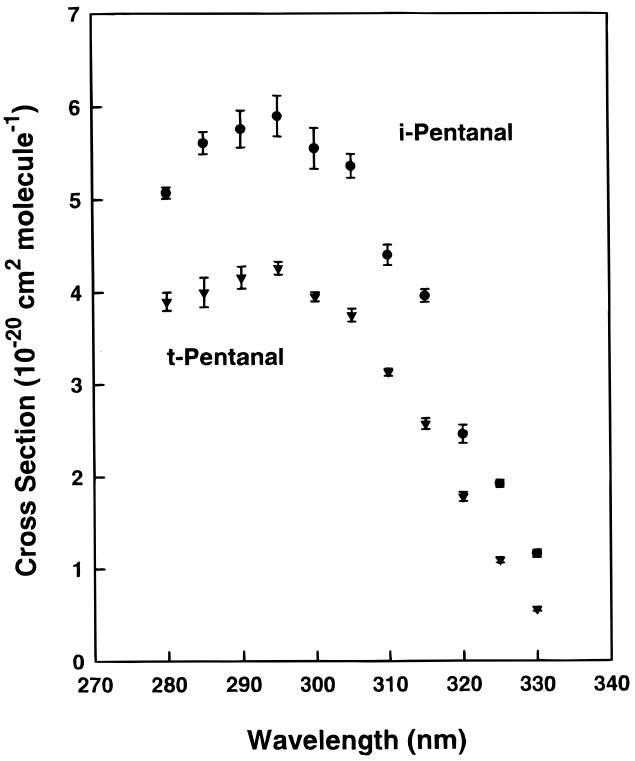

Figure 1. Room-temperature absorption cross-sections in the 280−330 nm region for i-pentanal (●) and t-pentanal (▼). Error bars are ± 1σ.

TABLE 1: Absorption Cross-Sections of i-Pentanal and t-Pentanal as a Function of Wavelength

λ (nm)	$\sigma_{\text{n-pentanal}}$ (10^{-20} cm^2)[a]	$\sigma_{\text{i-pentanal}}$ (10^{-20} cm^2)	$\sigma_{\text{t-pentanal}}$ (10^{-20} cm^2)
280	5.48 ± 0.15	5.07 ± 0.06	3.90 ± 0.10
285	6.23 ± 0.09	5.61 ± 0.12	4.00 ± 0.16
290	6.09 ± 0.15	5.76 ± 0.20	4.16 ± 0.12
295	6.56 ± 0.17	5.90 ± 0.22	4.26 ± 0.07
300	5.80 ± 0.16	5.55 ± 0.22	3.95 ± 0.05
305	5.43 ± 0.09	5.36 ± 0.13	3.75 ± 0.07
310	4.41 ± 0.07	4.40 ± 0.11	3.13 ± 0.04
315	3.74 ± 0.09	3.96 ± 0.07	2.57 ± 0.06
320	2.36 ± 0.10	2.46 ± 0.10	1.78 ± 0.05
325	1.81 ± 0.07	1.92 ± 0.04	1.09 ± 0.03
330	1.03 ± 0.15	1.16 ± 0.04	0.560 ± 0.023

[a] Reference 5.

Results and Discussion

Absorption Cross-Sections of i-Pentanal and t-Pentanal in the 280−330 nm Region. Figure 1 shows room-temperature absorption cross-sections of i-pentanal and t-pentanal in the 280−330 nm region. The absorption cross-section at each wavelength was obtained by monitoring the transmitted photolysis photon intensity as a function of i-pentanal or t-pentanal pressure in the cell and by applying Beer's law to the data obtained. Error bars quoted (1σ) represent the precision of the cross-section determinations and include the standard deviation for each measurement (~0.5%) plus the standard deviation about the mean of typically four repeated experimental runs. Systematic errors include those involving pressure (1%) and path length (0.2%) determinations. Taking together random errors (see Table 1 for i-pentanal and t-pentanal) and systematic errors, the overall uncertainty in cross-section measurements is ~5% for i-pentanal and t-pentanal in the 280−330 nm range. As seen from Figure 1, the absorption spectra of i-pentanal and t-pentanal showed little structure in the wavelength region studied. The magnitudes

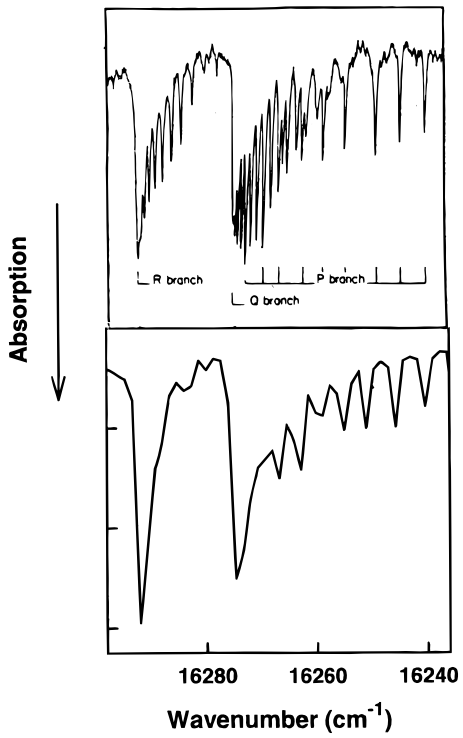

Figure 2. The lower trace is a low resolution cavity ring-down absorption spectrum of the product following the photolysis of 4 Torr t-pentanal at 295 nm. The upper trace is a time-resolved intracavity laser absorption spectrum of the $(00^10)\rightarrow(09^00)$ vibronic transition of HCO following the 266 nm photolysis of 0.1 Torr CH_3CHO and 10 Torr Ar (adapted from ref 20).

of the i-pentanal cross-sections were ~40% larger than those of t-pentanal in the 280−320 nm region, and the magnitude difference increased to about a factor of 2 at 325 and 330 nm. The smaller absorption cross-sections for t-pentanal might be explained in terms of increased aldehyde π^* energy brought about by the steric effect of the bulky *tert*-butyl group. Cross-section data for i-pentanal and t-pentanal (in units of cm^2 $molecule^{-1}$, base e) obtained from this study are tabulated in Table 1.

Time-Resolved Studies of Photolysis of i-Pentanal and t-Pentanal in the 280−330 nm Range. *Temporal Profiles of HCO from Photolysis of i-Pentanal and t-Pentanal.* Displayed in Figure 2 is a cavity ring-down absorption spectrum of the t-pentanal photolysis product measured at a pump/probe laser delay of 10 μs in the 613−616 nm range. Also shown in the same figure is a previously reported absorption spectrum[18−21] of HCO in the same wavelength region. A comparison of these two spectra shows that they are alike within the limits of resolution and indicates that HCO is a photodissociation product of t-pentanal. A similar product absorption spectrum was also obtained from i-pentanal photolysis. The cavity ring-down spectrometer was tuned to the HCO X $^2A''(0,0,0) \rightarrow \tilde{A}\ ^2A'$ (0,9,0) R bandhead at 613.8 nm, and the HCO concentration was followed as a function of time. Illustrated in Figure 3 is a time profile of the HCO radical generated from the 295 nm photolysis of t-pentanal, along with a fit of subsequent HCO decay by the following kinetic scheme:

$$HCO + HCO \rightarrow H_2CO + CO \quad (5)$$

$$HCO + t\text{-}C_4H_9 \rightarrow \text{products} \quad (6)$$

$$t\text{-}C_4H_9 + t\text{-}C_4H_9 \rightarrow C_8H_{18} \quad (7a)$$

$$\rightarrow i\text{-}C_4H_{10} + i\text{-}C_4H_8 \quad (7b)$$

This modeling scheme assumes that $t\text{-}C_4H_9 + HCO$ is the only important radical formation channel from photolysis around 300 nm. This assumption is supported by the approximate unity HCO quantum yield from the photolysis of t-pentanal described later in this section. Time-resolved HCO decay profiles from the photodissociation of 3, 6, and 9 Torr t-pentanal were compared with those calculated using the ACUCHEM simulation program. The following input parameters were used for the ACUCHEM program: rate constants for HCO + HCO, HCO + $t\text{-}C_4H_9$, and $t\text{-}C_4H_9$ + $t\text{-}C_4H_9$ reactions ($k_{HCO+HCO}$, $k_{HCO+t\text{-}C_4H_9}$, $k_{t\text{-}C_4H_9+t\text{-}C_4H_9}$), and HCO initial concentration ($[HCO]_0$). The rate constant for the recombination of $t\text{-}C_4H_9$ radicals, $k_{t\text{-}C_4H_9+t\text{-}C_4H_9}$ of 1.5×10^{-11} cm^3 $molecule^{-1}$ s^{-1}, was taken from the literature.[22] Initial estimates for $k_{HCO+HCO}$ and $k_{HCO+t\text{-}C_4H_9}$ were used in the ACUCHEM program and the simulated HCO decay profile was compared with that obtained from the experiments. The rate constants $k_{HCO+HCO}$ and $k_{HCO+t\text{-}C_4H_9}$ were then adjusted to obtain

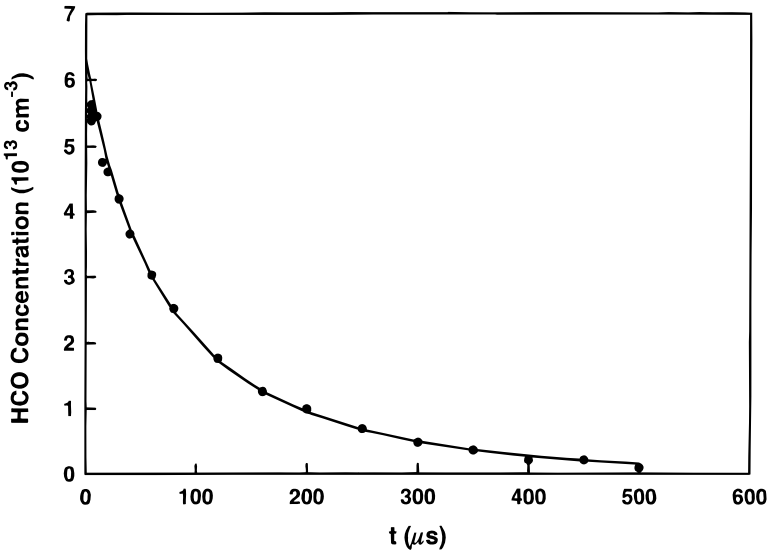

Figure 3. Time profile of the HCO radical decay from the photolysis of 6 Torr t-pentanal at 295 nm. Also shown is a fit of HCO decay using a kinetic model involving HCO + HCO, HCO + $t\text{-}C_4H_9$, and $t\text{-}C_4H_9$ + $t\text{-}C_4H_9$ reactions.

an optimum fit of the experimental data. Extracted rate constants were $(6.7 \pm 1.5) \times 10^{-11}$ and $(4.3 \pm 1.1) \times 10^{-11}$ cm^3 molecule^{-1} s^{-1} for $k_{HCO+HCO}$ and $k_{HCO+t\text{-}C_4H_9}$, respectively, where uncertainty (1σ) reflects experimental scatter only. Values of $k_{HCO+HCO}$ and $k_{HCO+t\text{-}C_4H_9}$ were affected by uncertainties in $[HCO]_0$ and the time resolution of the cavity ring-down technique ($\sim$12 μs around 613 nm). The time resolution of the cavity ring-down technique and the accuracy of $[HCO]_0$ were estimated to introduce a maximum uncertainty of 10% and 15% in both $k_{HCO+HCO}$ and $k_{HCO+t\text{-}C_4H_9}$, respectively. The overall uncertainty in the fitted value of $k_{HCO+HCO}$ and $k_{HCO+t\text{-}C_4H_9}$ including both random and systematic errors was $\sim$50%. The extracted $k_{HCO+HCO}$ and $k_{HCO+t\text{-}C_4H_9}$ rate constants agree well with the recommended rate constant for the HCO + HCO reaction[23] ($2.5 \times 10^{-11} \leq k \leq 10^{-10}$ cm^3 molecule^{-1} s^{-1} at 300 K) and the previously reported rate constant[24] for HCO + t-C_4H_9 reaction ($(4.7 \pm 1.1) \times 10^{-11}$ cm^3 molecule^{-1} s^{-1}). A similar procedure was used to extract $k_{HCO+i\text{-}C_4H_9}$ from time-dependent HCO profiles from the photolysis of i-pentanal. A rate constant value of $(6.2 \pm 1.5) \times 10^{-11}$ cm^3 molecule^{-1} s^{-1} was obtained for $k_{HCO+i\text{-}C_4H_9}$.

HCO Radical Yields from Photolysis of Pentanal. The yield of HCO was derived from the ratio of the HCO concentration produced in the photolysis/probe laser overlapping region to the absorbed photon density in the same region. The overlapping region could be viewed as a parallelepiped with width and height defined by those of the photolysis beam, and length defined by (beam width) $\times$ tan(15°)$^{-1}$, where 15° is the angle between the photolysis and the probe beams. Since the photolysis beam was absorbed by t-pentanal through the entire sidearm through which it traveled, absorption by t-pentanal in the photolysis/probe laser overlapping region was calculated from the difference in the transmitted photolysis photon energy at the beginning and at the end of the overlapping region. The photolysis photon energy into the cell was determined with a Joulemeter calibrated by acetone photolysis actinometry.[6] Its transmission loss at the front window of the cell ($\sim$8%) was corrected for. Once the absorption cross-section of t-pentanal at a given photolysis wavelength and the incident photon energy were known, the absorbed photon density in the region where the photolysis and probe beams overlapped could be calculated for a given initial t-pentanal pressure. The HCO concentration produced at a given photolysis wavelength was acquired by measuring HCO absorption at 613.8 nm at a photolysis to probe laser delay of 10 μs. To convert HCO absorption into absolute concentrations, the absorption cross-section of HCO at the probe laser wavelength was determined relative to the photolysis reaction $H_2CO + h\nu \rightarrow HCO + H$, for which the HCO quantum yield is known.[23] H_2CO was produced immediately prior to each calibration run in a glass bulb. The purity of H_2CO was estimated by comparing the absorption cross-section determined in the present study with literature values.[25,26] The H_2CO absorption cross-section was obtained by measuring the transmitted photolysis photon energy as a function of H_2CO pressure in the cell and by applying Beer's law to the data obtained. Except for 290 nm, our H_2CO cross-sections agreed within $\pm$15% with those obtained by Moortgat et al.[25] at $\lambda \leq 300$ nm. At 290 nm, an average of four cross-section measurements made over four samples and two different running days yielded an average H_2CO cross-section of $(6.05 \pm 0.60) \times 10^{-21}$ cm^2, which is about half of 1.30×10^{-20} cm^2 reported by Moortgat et al.[25] We attribute this difference to the fine structure in the H_2CO absorption spectrum. Cross-section data reported by Moortgat et al.[25] were centered at 290 nm and averaged over a 0.5 nm interval. In this work, our photolysis laser had a wavelength resolution of 0.15 cm^{-1}. Thus, our cross-section data reflect fine structure in the H_2CO absorption spectrum. In the 300−330 nm region, recommended H_2CO cross-sections[26] were low resolution data centered at different wavelengths than those used in the current study and were averaged over a 2.5 nm interval. Direct comparison was not made here.

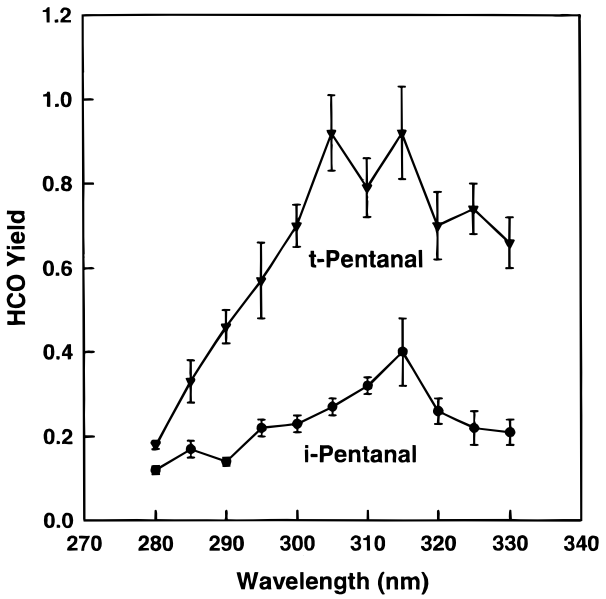

Figure 4. Wavelength-dependent HCO yields from photolysis of i-pentanal (●) and t-pentanal (▼). Error bars are $\pm 1\sigma$.

The HCO radical yield was determined from the photolysis of 0.5, 1, 2, 4, 6, 8, 10, and 12 Torr t-pentanal, and its dependence on t-pentanal pressure was examined. The HCO radical yield increased with t-pentanal pressure from 0.5 to 2 Torr. Since HCO yield was determined by monitoring the ground vibrational state of HCO at 10 μs after the photolysis pulse, we attribute this increase in HCO yield to vibrational relaxation of HCO from the excited states to the ground state. If the excited HCO radicals had not relaxed to the ground state at the detection time used, we would not be able to detect these radicals. Increasing t-pentanal pressure in the 0.5−2 Torr range speeds up vibrational relaxation of HCO. On the other hand, the extent of HCO + HCO, HCO + t-C_4H_9, and t-C_4H_9 + t-C_4H_9 reactions is different at 10 μs after photolyzing 2 versus 12 Torr of t-pentanal. After correcting for this difference in the extent of radical−radical reactions using HCO + HCO, HCO + t-C_4H_9, and t-C_4H_9 + t-C_4H_9 rate constants determined in this study, the HCO radical yield was found to be independent of t-pentanal pressure in the 2−12 Torr range at all photolysis wavelengths studied. The photolysis laser fluence was repeatedly monitored during the course of the HCO yield measurements so that the drop in laser fluence with time was corrected. Also the HCO yield at a given t-pentanal pressure was measured several times during the course of the experiments to ensure consistency of the results. Wavelength-dependent HCO radical yields thus obtained are plotted in Figure 4 and tabulated in Table 2. Errors quoted (1σ) are estimated based upon at least two experimental runs with approximately eight aldehyde pressures in each run. The absolute accuracy of HCO yield was affected by uncertainties in the determination of the following parameters: H_2CO concentration and absorption cross-section ($\sim$10% at 280−295, 305, 315−325 nm; 22% at 310 nm; 33% at 300 nm; 35% at 330 nm), t-pentanal absorption cross-section

TABLE 2: HCO Radical Yields of i-Pentanal and t-Pentanal as a Function of Wavelength

	φ_{HCO}		
λ (nm)	(n-pentanal)[a]	(i-pentanal)	(t-pentanal)
280	0.058 ± 0.006	0.12 ± 0.01	0.18 ± 0.01
285	0.095 ± 0.009	0.17 ± 0.02	0.33 ± 0.05
290	0.10 ± 0.02	0.14 ± 0.01	0.46 ± 0.04
295	0.14 ± 0.01	0.22 ± 0.02	0.57 ± 0.09
300	0.10 ± 0.02	0.23 ± 0.02	0.70 ± 0.05
305	0.15 ± 0.02	0.27 ± 0.02	0.92 ± 0.09
310	0.14 ± 0.02	0.32 ± 0.02	0.79 ± 0.07
315	0.20 ± 0.06	0.40 ± 0.08	0.92 ± 0.11
320	0.14 ± 0.02	0.26 ± 0.03	0.70 ± 0.08
325	0.085 ± 0.034	0.22 ± 0.04	0.74 ± 0.06
330	0.087 ± 0.015	0.21 ± 0.03	0.66 ± 0.06

[a] Reference 5.

(∼5% in the 280−330 nm region), pulse energy (5%), and dye laser width. To examine the effect of uncertainty in the measurement of photolysis laser width on HCO yield, HCO yield was computed using a photolysis beam width both of 0.15 and 0.20 cm. Since HCO yield from photodissociation of t-pentanal was determined relative to that from photodissociation of formaldehyde, HCO yield was found to be the same when the beam width was varied from 0.15 to 0.20 cm. Taking together random and systematic errors, the overall uncertainties in HCO yield measurements are ∼25% at 280 nm; ∼30% at 290, 305, 315−325 nm; ∼35% at 285, 295 nm; ∼40% at 310 nm; ∼50% at 300 nm; ∼55% at 330 nm. As seen from Figure 4, HCO yields exhibit dramatic dependence on photolysis wavelength. The HCO yields were close to unity in the 305−315 nm range and then decreased at both longer and shorter wavelengths. The near unity HCO yield in the 305−315 nm region suggests that formation of HCO + t-C_4H_9 was the dominant t-pentanal photodissociation pathway. The decrease in HCO yields at shorter photolysis wavelength can possibly be attributed to the opening up of a molecular elimination channel (i-C_4H_{10} + CO) at higher photon energies. The reduced HCO yield at the longer wavelength tail was probably a consequence of photodissociation at near-threshold wavelengths.

The effect of total pressure on HCO radical yields was measured at 280, 295, 310, and 325 nm by maintaining constant t-pentanal pressure (2 Torr) and varying nitrogen carrier gas pressure. The HCO radical yields were found to be independent of total pressure when total pressure was varied between 20 and 400 Torr at the photolysis wavelengths studied.

HCO Radical Yields from Photolysis of i-Pentanal. A similar procedure as described above was used to determine HCO radical yields from photolysis of 2, 4, 6, 8, 10, and 12 Torr of i-pentanal. Because of the smaller HCO radical yields, and thus the smaller HCO signal size at lower i-pentanal pressures, photodissociation was not conducted at an i-pentanal pressure less than 2 Torr. The dependence of HCO yield on i-pentanal pressure was studied. After correcting for the difference in the extent of HCO + HCO, HCO + i-C_4H_9, i-C_4H_9 + i-C_4H_9 radical reactions at 10 μs after photolyzing 2, 4, 6, 8, 10, and 12 Torr i-pentanal, the HCO radical yield in the 280−325 nm range was found to be independent of i-pentanal pressure within experimental error limits. At 330 nm, HCO yields decreased with increasing i-pentanal pressure. Since 330 nm is close to the threshold wavelength (calculated threshold = 340 nm) for photodissociation of i-pentanal, increasing i-pentanal pressure apparently quenched the excited-state i-pentanal to below its dissociation threshold. Variation of HCO yield with wavelength thus obtained was plotted in Figure 4 and listed in Table 2. Errors quoted (1σ) reflect experimental scatter and were derived from at least two experimental runs with about six aldehyde pressures per run. Estimated uncertainties in the determination of the following parameters are as follows: H_2CO concentration and absorption cross-section (∼10% at 280, 285, 300−310, 325 nm; ∼15% at 290, 295, 315 nm; ∼34% at 320, 330 nm), i-pentanal absorption cross-section (∼5% in the 280−330 nm region), and pulse energy (5%). The overall uncertainty in HCO yield measurements including both random and systematic errors are ∼25% at 305, 310 nm; ∼30% at 280−290, 300 nm; ∼35% at 295 nm; ∼40% at 325 nm; ∼45% at 315 nm; ∼55% at 320 nm; ∼60% at 330 nm. As can be seen from Figure 4, HCO yield from the photolysis of i-pentanal displayed significant wavelength dependence and decreased at both the longer and the shorter wavelength tails. The HCO radical yields exhibit a maximum of 0.40 ± 0.08 at 315 nm.

The variation of HCO yields with total pressure was examined at 280, 295, 310, and 325 nm by keeping i-pentanal pressure the same and changing nitrogen carrier gas pressure. Total pressure was varied between 20 and 400 Torr at the wavelengths studied. The HCO yield was found to be independent of total pressure at 280, 295, and 310 nm. At 325 nm, HCO yield decreased by ∼25% when total pressure was increased from 20 to 400 Torr. This observation is consistent with the notion that increased molecular collisions, owing to increased pressure, quench the HCO yield near the threshold of i-pentanal photolysis.

Comparison of HCO Quantum Yields from n-, i-, and t-Pentanal Photolysis. HCO radical yields exhibited significant wavelength variation from photolysis of n-, i-, and t-pentanal. The decay in HCO yields was observed both at the longer and at shorter wavelength tails for all three molecules. The magnitude of the maximum HCO yield was very different for the photodissociation of n-, i-, and t-pentanal (0.20, 0.40, and 0.92 at 315 nm, respectively). An HCO yield of close to unity was obtained from the photolysis of t-pentanal in the 305−315 nm range. Since the Norrish II type process is unavailable from t-pentanal photolysis, the formation of HCO + t-C_4H_9 is the predominant photofragmentation pathway around 310 nm. Our previous study[5] on the photolysis of n-pentanal indicates that the quantum yield of the Norrish II process ($\varphi_{CH_3CHO} \sim 0.9$) is much larger than the yield of the radical formation channel ($\varphi_{HCO} = 0.14 \pm 0.02$) at 310 nm. Thus, the Norrish II process appears to take place at the expense of the radical formation channel in the case of n-pentanal photolysis. The HCO yields from the photolysis of i-pentanal were smaller than those obtained from t-pentanal photolysis but were larger by a factor of 1.4−2.6 than those obtained from n-pentanal photolysis. The Norrish II process is less favored for i-pentanal than for n-pentanal because the transition state involves breaking a stronger primary C−H bond rather than a secondary C−H bond. As a result, HCO radical yields from i-pentanal photolysis were larger than those obtained from n-pentanal photolysis.

End Product Studies. i-Pentanal and t-pentanal were photolyzed in a closed cell at 290, 310, and 330 nm in the presence of nitrogen. The DNPH-derivatized aldehyde products were measured by HPLC. i-Pentanal, t-pentanal, and nitrogen pressures of 10, 10, and 160 Torr, respectively, were used in the experiments. For t-pentanal photolysis, the only aldehyde product observed was formaldehyde which is possibly formed from the HCO + HCO recombination reaction (reaction 5). The lack of acetaldehyde product from t-pentanal photodissociation is consistent with the near unity HCO radical yield in the 305−315 nm region and the unavailability of the Norrish II channel. Acetaldehyde was detected by HPLC after photolysis of an

TABLE 3: Photolysis Rate Constants Leading to the Formation of the HCO Radical

	k_{rad}		
	(n-pentanal)[a]	(i-pentanal)[a]	(t-pentanal)[a]
January 1	1.1×10^{-5}	2.6×10^{-5}	4.5×10^{-5}
July 1	3.8×10^{-5}	8.3×10^{-5}	1.5×10^{-4}

[a] In units of s^{-1}.

i-pentanal/N_2 mixture. This suggests the occurrence of the Norrish II photodissociation channel

$$(CH_3)_2CHCH_2CHO + h\nu \rightarrow CH_3CH{=}CH_2 + CH_3CHO \quad (8)$$

Quantum yields of aldehydes from the photolysis of an i-pentanal/N_2 mixture were estimated from the conservation of total carbonyls before and after photodissociation. Less than 5% of i-pentanal was photolyzed in the experiments. If we assume all of the carbonyl groups from the photolysis of an i-pentanal/N_2 mixture existed as aldehydes and were detected by HPLC, individual aldehyde percentages on the chromatogram can be estimated by summing the peak areas of all the aldehydes and dividing the individual aldehyde peak area by the sum. The amount of individual aldehyde produced from photodissociation was determined from the ratio of its peak area to total peak area after photolysis. The amount of i-pentanal photolyzed was obtained from the difference in the chromatogram i-pentanal percentage before and after photolysis. The individual aldehyde yield was acquired by dividing the amount of aldehyde formed by the amount of i-pentanal photolyzed. Since carbonyl groups from photofragmentation of an i-pentanal/N_2 mixture may also exist as CO, which was not detected by HPLC, this analysis only provided a crude estimate of aldehyde yields. The acetaldehyde quantum yields thus obtained are $\sim$ 50%, 65%, and 60% at 290, 310, and 330 nm, respectively.

Photodissociation Rate Constant to Form HCO Radicals in the Atmosphere. The photodissociation rate constants (k_{rad}) for HCO production (or HO_2 production in the presence of air) from i-pentanal and t-pentanal photolysis were calculated from the actinic solar flux ($J(\lambda)$) reported by Demerjian et al.,[27] the i-pentanal or t-pentanal absorption cross-section ($\sigma(\lambda)$), and HCO radical yield ($\Phi(\text{rad}, \lambda)$) using the relationship

$$k_{rad} = \int \sigma(\lambda) \cdot \Phi(\text{rad},\lambda) \cdot J(\lambda) \mathrm{d}\lambda \quad (9)$$

Under cloudless conditions at sea level and a latitude of 40° N, the photolysis rate constants for i-pentanal and t-pentanal to form HCO are 2.6×10^{-5} s^{-1} and 4.5×10^{-5} s^{-1}, respectively, for noontime on January 1, and 8.3×10^{-5} s^{-1} and 1.5×10^{-4} s^{-1}, respectively, for noontime on July 1. Calculated photolysis rate constants for i-pentanal and t-pentanal are listed in Table 3 along with those for n-pentanal. For the purpose of comparison, acetaldehyde photodissociation rate constants that lead to radical formation were computed. They are 6.1×10^{-6} s^{-1} for January 1 and 2.5×10^{-5} s^{-1} for July 1. The calculated radical formation rate constants from i-pentanal and t-pentanal photolysis are 4.3 and 7.4 times those obtained from acetaldehyde photolysis for the January 1 condition, and 3.3 and 6.0 times those obtained from acetaldehyde photolysis for the July 1 condition.

Acknowledgment. We thank undergraduate assistants, Mr. Andrew Levine and Mr. Vu Q. Huynh, for their assistance in the experiments. The major portion of this work was supported by the National Science Foundation under Grant No. ATM-9610285. Student assistants were supported by the Petroleum Research Fund under Grant No. 32261-AC6.

References and Notes

(1) Graedel, T. E.; Farrow, L. A.; Weber, T. A. *Atmos. Environ.* **1976**, *10*, 1095.
(2) Grosjean, D. *Environ. Sci. Technol.* **1982**, *16*, 254.
(3) Finlayson-Pitts, B. J.; Pitts, J. N., Jr. *Atmospheric Chemistry*, John Wiley: New York, 1986.
(4) Lloyd, A. C. *NBS Spec. Publ.* **1979**, *557*, 27.
(5) Cronin, T. J.; Zhu, L. *J. Phys. Chem.* **1998**, *102*, 10274.
(6) Calvert, J. G.; Pitts, J. N., Jr. *Photochemistry*, John Wiley: New York, 1966.
(7) Lee, E. K. C.; Lewis, R. S. *Adv. Photochem.* **1980**, *12*, 1.
(8) ΔH^0_f of -236.5 kJ/mol and -249.6 kJ/mol for i-pentanal and t-pentanal were taken from *TRC Thermodynamic Tables*, Thermodynamic Research Center, The Texas A & M University System, College Station, Texas, 1999.
(9) *CRC Handbook of Chemistry and Physics*, CRC Press: Boca Raton, Florida, 1997.
(10) Seetula, J. A.; Slagle, I. R. *J. Chem. Soc., Faraday Trans.* **1997**, *93*, 1709.
(11) Birrell, R. N.; Trotman-Dickenson, A. F. *J. Chem. Soc.* **1960**, 4218.
(12) Bamford, C. H.; Norrish, R. G. W. *J. Chem. Soc.* **1935**, 1504.
(13) O'Keefe, A.; Deacon, D. A. G. *Rev. Sci. Instrum.* **1988**, *59*, 2544.
(14) O'Keefe, A.; Scherer, J. J.; Cooksy, A. L.; Sheeks, R.; Heath, J.; Saykally, R. J. *Chem. Phys. Lett.* **1990**, *172*, 214.
(15) Zhu, L.; Johnston, G. *J. Phys. Chem.* **1995**, *99*, 15114.
(16) Zhu, L.; Kellis, D.; Ding, C.-F. *Chem. Phys. Lett.* **1996**, *257*, 487.
(17) Moortgat, G.; Warneck, P. *J. Chem. Phys.* **1979**, *70*, 3639.
(18) Herzberg, G.; Ramsay, D. A. *Proc. R. Soc. (London)* **1955**, *A233*, 34.
(19) Johns, J. W. C.; Priddle, S. H.; Ramsay, D. A. *Discuss. Faraday Soc.* **1963**, *35*, 90.
(20) Stoeckel, F.; Schuh, M. D.; Goldstein, N.; Atkinson, G. H. *Chem. Phys.* **1985**, *95*, 135.
(21) Reilly, J. P.; Clark, J. H.; Moore, C. B.; Pimentel, G. C. *J. Chem. Phys.* **1978**, *69*, 4381.
(22) Parkes, D. A.; Quinn, C. P. *J. Chem. Soc., Faraday Trans. 1* **1976**, *72*, 1952.
(23) Atkinson, R.; Baulch, D. L.; Cox, R. A.; Hampson, R. F., Jr.; Kerr, J. A.; Troe, J. *J. Phys. Chem. Ref. Data* **1992**, *21*, 1125.
(24) Baggott, J. E.; Frey, H. M.; Lightfoot, P. D.; Walsh, R. *J. Phys. Chem.* **1987**, *91*, 3386.
(25) Moortgat, G. K.; Seiler, W.; Warneck, P. *J. Chem. Phys.* **1983**, *78*, 1185.
(26) Cantrell, C. A.; Davidson, J. A.; McDaniel, A. H.; Shetter, R. E.; Calvert, J. G. *J. Phys. Chem.* **1990**, *94*, 3902.
(27) Demerjian, K. L.; Schere, K. L.; Peterson, J. T. *Adv. Environ. Sci. Technol.* **1980**, *10*, 369.